Toward the Design of Chlorine Soft Sensors via Stepwise Safe Switching Observers for a Primary Water Distribution Network

Nikolaos D. Kouvakas [0000-0001-5126-5226], Fotis N. Koumboulis [0000-0002-9856-049X], Maria P. Tzamtzi [0009-0008-8930-1024] and Dimitrios G. Fragkoulis [0000-0002-0177-5110]

Robotics, Automatic Control and Cyber-Physical Systems Laboratory, Department of Digital Industry Technologies, School of Science, National & Kapodistrian University of Athens, Euripus Campus, 34400, Greece

nkouvak@dind.uoa.gr, fkoumboulis@dind.uoa.gr, mtzamtzi@dind.uoa.gr, dfragkoulis@dind.uoa.gr

Abstract. In the present paper the problem of designing chlorine soft sensors via safe switching observers for primary water distribution networks is investigated. A primary water distribution network benchmark is studied. First, it is modelled as a system of nonlinear hyperbolic partial differential equations describing fluid motion in the pipe network and a set of partial differential equations describing advection, dispersion and decay of chlorine in the pipes. The model of the network incorporates water demand from users. The overall model is approximated as a system of nonlinear ordinary differential equation. Based on the nonlinear approximation of the network, linear approximants, around prespecified operating points, are produced. Based on this set of operating points a bank of switching linear observers is developed toward estimation of chlorine concentration at specific points of interest. The observer parameters are determined via a combined pole allocation and metaheuristic algorithm. The design is completed through a data-driven rule-based system, performing stepwise switching between the observers of the bank, for the operating points determined previously. The efficiency of the proposed switching scheme is demonstrated through series of computational experiments, where it is observed that the proposed approach performs satisfactorily.

Keywords: Water Distribution Networks, Water Quality, Soft Sensor Design.

1 Introduction

Compared to traditional hardware sensors, which are expensive to install and maintain, soft sensors employ system models, AI tools and measurable variable to estimate unmeasured variables in real time. See [1] and [2] as well as the references therein. Soft Sensors possess several advantages: reduction of infrastructure cost and provision of estimates physical quantities even when direct measurement is not feasible. Moreover, soft sensors enhance resilience in systems through continuous monitoring and fault detection as well as predictive analysis, and hence are suitable for complex water infrastructure setups.

Soft sensors can be an increasingly valuable tools for flow and quality variable estimation in Water Distribution Networks (WDNs). Of particular interest is the use artificial intelligence approaches for the estimation of quality and flow parameters. Indicatively see [3]-[8] and the references therein. In [3], an LSTM-based neural network soft sensor with Monte Carlo dropout for predicting flow rates in water supply systems has been proposed. The soft sensor has improved accuracy and reduced uncertainty as compared to other models. The goal of this approach was to enhance efficiency and cost-effectiveness by minimizing water losses through precise flow estimation. In [4], an ANN-based soft sensor integrated with a digital twin of a WDN has been introduced. The goal was to enable accurate parameter estimation across the network using minimal physical sensors. Trained on CFD data, the model has achieved accuracy and offered a cost-effective solution for real-time monitoring and proactive maintenance. In [5], a soft sensor for estimating flow in water supply systems, using an artificial neural network, has been presented. In [6], a soft sensor for chlorine-based water quality monitoring and using extreme learning machine techniques has been proposed. The ELM-based model used in this study has proved efficiency and accuracy as compared to SVM approaches. In [7], an intelligent inference engine for real-time water quality assessment and prediction in urban water system has been proposed. This system used machine learning algorithms to estimate pH and dissolved oxygen. In [8], a dynamic, data-driven soft sensor model for real-time turbidity prediction in drinking water has been presented. The goal of the approach was to enhance online monitoring and identify key variables influencing turbidity.

Another category of soft sensors is that based on observer design. Observer based approaches have been proposed to estimate mainly hudraulic characteristics of WDNs. Indicatively see [9] to [13] and the references therein. In [9], an online method, using a nonlinear state observer, has been proposed. The goal of the study is to continuously estimate pipe roughness in WDNs by modeling the system as a network of damped nonlinear oscillators. The approach relies solely on flow rate data and enables real-time calibration to support improved operational tasks like control and diagnostics. In [10], an interval-based hydraulic state estimation algorithm for leakage detection in urban WDNs has been proposed. The method is efficient for unstructured uncertainties in demand and network parameters and is demonstrated on benchmark scenarios. In [11], a recursive estimation algorithm for jointly estimating variables and parameters in drinking water distribution systems has been proposed. The estimation has focused on both water quantity and quality and incorporates dynamic grid design for efficient piecewise linearization of nonlinear models. In [12], the problem of multi-leak diagnosis in branched pipeline networks has been investigated, by combining k-NN based leak region classification with Extended Kalman Filters. The approach has been validated experimentally on a test bed. In [13], a leak detection and isolation method has been proposed for pipelines. The method fuses steady-state estimation with an Extended Kalman Filter, using pressure and flow data from pipeline ends.

In the present paper, the design of chlorine soft sensors for primary WDNs, using a safe switching observer approach, has been proposed for the first time. The primary

WDN is modeled by a set of nonlinear hyperbolic partial differential equations (PDEs) that govern fluid dynamics within the pipe network, alongside additional PDEs representing the advection, dispersion, and decay of chlorine. The model also accounts for user water demand. To facilitate observer design, the PDE-based model is approximated by a nonlinear system of ordinary differential equations (ODEs). Linearized models are then generated around selected operating points, forming the basis for a bank of switching linear observers tasked with estimating chlorine concentration at designated locations within the network. The parameters of these observers are optimized using a metaheuristic algorithm. Finally, a data-driven, rule-based switching mechanism is employed to select the appropriate observer based on the current operating condition. The effectiveness of the proposed observer design is validated through computational experiments, demonstrating its satisfactory performance.

The present approach as compared to to single-step linear observers, is more effectivve and accurate in the sense that Single operating point observers are in general poor at describing dynamic behavior when the system moves away from the operating point and provide large estimation errors. Switching between locally valid observers avoids this deawback by using each observer, inside its region of validity, indicatively see [1] and [2]. In contrast to nonlinear observers, indicatively see [14], the switching approach of linear observers is less sensitive to parameter changes and noise, as well as more resilient towards model uncertainties. Nonlinear observers, although they are theoretically capable to estimate system dynamics, are subject to requiring precise information of the system and are prone to divergence when exposed to actual-world disturbances or model errors. The linear switching observer avoids these issues by leveraging powerful, traditional linear design techniques in each operating mode, with the inclusion of an analyzable switching logic. Further, comparing the present method with machine learning estimation methods [15]-[17], it is remarked that the method at hand provides interpretability, convergence guarantees, and reliability. Additionally, machine learning methods operate in general as black box methods and their results depend upon the training data set. They also typically require significant computational resources. In contrast, the method at hand, that belongs in the general family of artificial intelligence methods, is transparent and less computationally intensive.

2 Water Distribution Network Modeling

2.1 Flow Rate, Pressure Head and Clorine Decay in a Closed Conduit

Following the trend, in the literature (see [18] and the references therein), in order to compute the transient flow in a closed conduit, the following assumptions are made:

a) Each pipe is straight and free of fittings or slope.
b) The fluid exhibits slight compressibility.
c) The duct walls are slightly flexible.
d) Variations in convective velocity are negligible.
e) The duct maintains a constant cross-sectional area.

f) The fluid density and viscosity remain constant.

Based on the above assumptions, the transient state of the flow in a pipeline is described by the following set of hyperbolic partial differential equations (see [18]):

$$\frac{\partial H(z,t)}{\partial t}+\frac{b^2}{gA}\frac{\partial Q(z,t)}{\partial z}=0\,, \tag{1}$$

$$\frac{\partial Q(z,t)}{\partial t}+gA\frac{\partial H(z,t)}{\partial z}+\frac{f(Q,D,\varepsilon)}{2DA}Q(z,t)\left|Q(z,t)\right|=0\,, \tag{2}$$

where Q denotes the volumetric flow rate in the pipeline, H is the corresponding pressure head, z is the spatial coordinate, t denotes time, g is the gravitational acceleration, A is the cross-sectional area of the pipe, b is the speed of the pressure wave, D is the inner pipe diameter, f is the friction coefficient and ε is the relative roughness of the pipe. Regarding the friction factor, three types of flow can be distinguished: a) laminar flow, b) transient flow, and c) turbulent flow. The type of flow depends upon the value of the Reynolds number (Re) [19], where $\mathrm{Re}=\frac{\rho v D}{\mu}$ and where ρ is the density of the fluid, v is the advective velocity of the fluid and μ is the dynamic viscosity of the fluid. Note that the advective velocity of the fluid is related to the volumetric flow rate as follows

$$Q=\frac{v\pi D^2}{4}\,. \tag{3}$$

Solving (3) with respect to the velocity, the Reynolds number can be expressed with respect to the volumetric flow rate as follows $\mathrm{Re}=\frac{4\rho Q}{\pi D\mu}$. If $0<\mathrm{Re}<2000$, then the fluid flow is characterized as laminar (see [20]). If $2000\le\mathrm{Re}\le 4000$, then the fluid flow is characterized as transient, while if $\mathrm{Re}>4000$ the flow is characterized as turbulent. If fluid flow is turbulent, which is the most common scenario for large-scale networks, the friction coefficient will be approximated [21] by the formula

$$f(Q,D,\varepsilon)=\lambda_1\log_{10}\left(\frac{\lambda_2}{\mathrm{Re}}+(\varepsilon/\lambda_3)^{\lambda_4}\right)^{-2}, \tag{4}$$

where $\lambda_j\in\mathbb{R}^+$ ($j=1,\ldots,4$).

Chlorine is commonly used for water disinfection to ensure microbiological safety in drinking water systems. Chlorine concentration decays with time and distance due to reactions with pipe wall, organic matter and other materials. Proper modeling of this decay is crucial to maintain water quality in a drinking water system. The dynamics of chlorine within water conduits will be expressed through a PDE of the form (see [22])

$$\frac{\partial c(z,t)}{\partial t}+v\frac{\partial c(z,t)}{\partial z}=M\frac{\partial^2 c(z,t)}{\partial z^2}-k_1 c(z,t)\,, \tag{5}$$

where c denotes constituent concentration, M is the dispersion coefficient and k_1 is the first order reaction rate, here considered to be constant. Considering that the flow in conduits is mainly affected by advection and that diffusion's role is insignificant, the diffusion term in (5) can be omitted to become

$$\frac{\partial c(z,t)}{\partial t}+v\frac{\partial c(z,t)}{\partial z}+k_1 c(z,t)=0\,. \tag{6}$$

Using (3), relation (6) takes on the form

$$\frac{\partial c(z,t)}{\partial t}+\frac{4Q(z,t)}{\pi D^2}\frac{\partial c(z,t)}{\partial z}+k_1 c(z,t)=0\,. \tag{7}$$

2.2 A Benchmark Branched Water Distribution Network

In the present section, the dynamic model of a benchmark water distribution network will be developed, based on the results of Subsections 2.1 and 2.2. The network (see Fig. 1) will be consisting of a main line with one branch, three reservoirs providing variable / actuatable head pressure to the network and water demand, acting as measurable disturbance, to unmodelled parts of the network. The network is similar to that presented in [23].

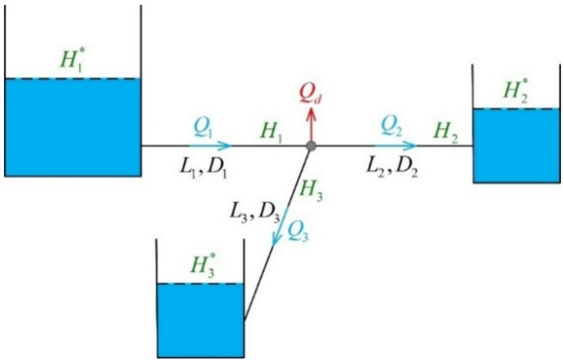

Fig. 1. Water distribution network setup.

Using the results of the previous subsections, the dynamics of the WDN in Figure 1 can described by the following set of equations

$$\frac{\partial H_j(z,t)}{\partial t}+\frac{b^2}{gA_j}\frac{\partial Q_j(z,t)}{\partial z}=0\,, \tag{8}$$

$$\frac{\partial Q_j(z,t)}{\partial t}+gA_j\frac{\partial H_j(z,t)}{\partial z}+\frac{f(Q_j,D_j,\varepsilon_j)}{2D_jA_j}Q_j(t)\left|Q_j(t)\right|=0\,, \tag{9}$$

$$\frac{\partial c_j(z,t)}{\partial t}+\frac{4Q_j(z,t)}{\pi D_j^2}\frac{\partial c_j(z,t)}{\partial z}+k_1 c_j(z,t)=0\,, \tag{10}$$

where Q_j, H_j and c_j ($j=1,2,3$) are the volumetric flow rates, pressures and chlorine concentrations in the respective pipes while D_j and ε_j denote the respective pipe diameters and relative roughness. For $j=1$ the spatial coordinate is bounded by $z\in[0,L_1]$, for $j=2$ the spatial coordinate is bounded by $z\in[0,L_2]$, while for $j=3$ the spatial coordinate is bounded by $z\in[0,L_3]$, where L_1, L_2 and L_3 are the lengths of conduits 1, 2 and 3 respectively. For the equations (8) to (10), to accurately represent the network presented in Fig. 1, the following boundary conditions and algebraic constraints are imposed

$$H_1(0,t)=H_1^*(t),\ H_2(L_2,t)=H_2^*(t),\ H_3(L_3,t)=H_3^*(t)\,,$$
$$H_1(L_1,t)=H_2(0,t)=H_3(0,t)=H_n^*(t)\,,$$
$$c_1(0,t)=c_1^*(t),\ c_2(L_2,t)=c_2^*(t),\ c_3(L_3,t)=c_3^*(t)\,,$$
$$Q_1(L_1,t)=Q_2(0,t)+Q_3(0,t)+Q_d(t)\,,$$

where H_1^*, H_2^* and H_3^* denote head pressures at reservoirs 1,2 and 3 respectively, c_1^*, c_2^* and c_3^* denote chlorine concentrations at reservoirs 1,2 and 3, respectively, and where H_n^* denotes pressure in the junction / node. The last algebraic constraint, regarding, the volumetric flow rates implies that the flow inside conduit 1 goes into the junction while the flows inside conduits 2 and 3 and the demand flow Q_d leave the junction. A negative value for Q_1, Q_2 or Q_3 implies reversal of the direction of the flow than the one presented in Fig. 1. The demand flow Q_d is considered to be greater than or equal to zero. Based on the assumption of complete mixing in any negligible node volume, it holds that $c_1(L_1,t)=c_2(0,t)=c_3(0,t)=c_n^*(t)$. Clearly, if the flow in a conduit moves toward the reservoir, then the chlorine concentration in the reservoir does not enter the network and the respective variable does not appear in the model.

2.3 Approximation of the Model of a Water Distribution Network through Systems of ODEs

Toward solution of the system of PDEs modelling a water distribution network, several approaches have been proposed. Of particular interest is the approach presented in [23], where a finite difference approach is used to discretize, with respect to the spatial coordinate only, the PDEs in (8) to (10), thus resulting in a set of ODEs. The resulting formulation offers significant advantages, especially for controller design and other related applications. Let

$$\left.\frac{\partial H(z,t)}{\partial z}\right|_{z=z_i} \simeq \frac{H_{i+1}(t)-H_i(t)}{\Delta z_i} \ ; \ i=1,\ldots,n , \tag{11}$$

$$\left.\frac{\partial Q(z,t)}{\partial z}\right|_{z=z_{i-1}} \simeq \frac{Q_i(t)-Q_{i-1}(t)}{\Delta z_{i-1}} \ ; \ i=2,\ldots,n , \tag{12}$$

$$\left.\frac{\partial c(z,t)}{\partial z}\right|_{z=z_i} \simeq \frac{c_i(t)-c_{i-1}(t)}{\Delta z_{i-1}} ; \ i=1,\ldots,n , \tag{13}$$

where n is the number of sections, z_k is the spatial coordinate of section k and $\Delta z_k = z_{k+1} - z_k$ denotes the k section length between two successive points of position z_{k+1} and z_k. For any particular pipe it holds that $z_1 = 0$, $z_{n+1} = L$ and z_k, for every k not equal to 1 or $n+1$, denotes an interior pipe point. Using the approximations in (11) to (13), a finite dimensional set of ODEs of the following form is derived

$$\frac{dQ_i(t)}{dt} = -\frac{gA}{\Delta z_i}\left(H_{i+1}(t)-H_i(t)\right) - \frac{f(Q_i,D_i,\varepsilon_i)}{2DA}Q_i(t)\left|Q_i(t)\right| \ ; \ i=1,\ldots,n , \tag{14}$$

$$\frac{dH_{i+1}(t)}{dt} = -\frac{b^2}{\Delta z_i g A_i}\left(Q_{i+1}(t)-Q_i(t)\right) \ ; \ i=1,\ldots,n-1 , \tag{15}$$

$$\frac{dc_{i+1}(t)}{dt} = -\left(\frac{4Q_i(t)}{\Delta z_{i+1}\pi D^2}+k_1\right)c_{i+1}(t) + \frac{4Q_i(t)}{\Delta z_{i+1}\pi D^2}c_i(t) \ ; \ i=0,\ldots,n-1 . \tag{16}$$

Here, the modelling of WDNs is based on the following four assumptions:

i. the friction coefficient follows formula (4),
ii. the flow in the conduits is slowly varying and that the flow variables can be discretized in space using a single step,
iii. the PDEs describing chlorine concentrations are divided into n_{cl} sections, and
iv. the flows in the conduit do not change directions.

The fourth assumption is reasonable and common, particularly for primary WDNs, where the network is typically laid out to have unidirectional flow under normal operating conditions. The main role of primary WDNs is to convey large volumes of water from purification plants to storage reservoirs or secondary distribution networks. The conveyance is often accomplished through pipelines that are pressurized and sized to provide stable flow paths.

Based on the above assumptions and applying a series of manipulations on (14) to (16), the ODE approximation of water distribution network in Figure 1, takes on the form

$$\frac{dQ_1}{dt} = \frac{A_1 g\left(H_1^* - H_n^*\right)}{L_1} - \frac{f(Q_1,D_1,\varepsilon_1)}{2A_1 D_1}Q_1^2 , \ \frac{dQ_2}{dt} = \frac{A_2 g\left(H_n^* - H_2^*\right)}{L_2} - \frac{f(Q_2,D_2,\varepsilon_2)}{2A_2 D_2}Q_2^2 ,$$

$$\frac{dQ_3}{dt}=\frac{A_3 g\left(H_n^*-H_3^*\right)}{L_3}-\frac{\left(Q_3,D_3,\varepsilon_3\right)}{2A_3D_3}Q_3^2,\ \frac{dH_n^*}{dt}=\frac{b^2}{L_1A_1g}\left(Q_1-Q_2-Q_3-Q_d\right),$$
$$\frac{dc_{1,1}}{dt}=\frac{4n_{cl}Q_1\left(c_{1,0}-c_{1,1}\right)}{L_1D_1^2\pi}-k_1c_{1,1},\ \frac{dc_{1,2}}{dt}=\frac{4n_{cl}Q_1\left(c_{1,1}-c_{1,2}\right)}{L_1D_1^2\pi}-k_1c_{1,2},$$
$$\frac{dc_{1,3}}{dt}=\frac{4n_{cl}Q_1\left(c_{1,2}-c_{1,3}\right)}{L_1D_1^2\pi}-k_1c_{1,3},\ \frac{dc_{2,1}}{dt}=\frac{4n_{cl}Q_2\left(c_{1,3}-c_{2,1}\right)}{L_2D_2^2\pi}-k_1c_{2,1},$$
$$\frac{dc_{2,2}}{dt}=\frac{4n_{cl}Q_2\left(c_{2,1}-c_{2,2}\right)}{L_2D_2^2\pi}-k_1c_{2,2},\ \frac{dc_{2,3}}{dt}=\frac{4n_{cl}Q_2\left(c_{2,2}-c_{2,3}\right)}{L_2D_2^2\pi}-k_1c_{2,3},$$
$$\frac{dc_{3,1}}{dt}=\frac{4n_{cl}Q_3\left(c_{1,3}-c_{3,1}\right)}{L_3D_3^2\pi}-k_1c_{3,1},\ \frac{dc_{3,2}}{dt}=\frac{4n_{cl}Q_3\left(c_{3,1}-c_{3,2}\right)}{L_3D_3^2\pi}-k_1c_{3,2},$$
$$\frac{dc_{3,3}}{dt}=\frac{4n_{cl}Q_3\left(c_{3,2}-c_{3,3}\right)}{L_3D_3^2\pi}-k_1c_{3,3}.$$

The constant flow direction condition implies that

$$\left(Q_1\geq 0\right)\wedge\left(Q_2\geq 0\right)\wedge\left(Q_3\geq 0\right)\wedge\left(Q_d\geq 0\right). \tag{17}$$

Let

$$x=\begin{bmatrix}x_1 & \cdots & x_{13}\end{bmatrix}^T=\left[Q_1\quad Q_2\quad Q_3\quad H_n^*\quad c_{1,1}\quad c_{1,2}\quad c_{1,3}\quad c_{2,1}\quad c_{2,2}\quad c_{2,3}\ \right.\vdots$$
$$\vdots\left.\ c_{3,1}\quad c_{3,2}\quad c_{3,3}\right]^T,\ u=\begin{bmatrix}u_1 & \cdots & u_5\end{bmatrix}^T=\begin{bmatrix}H_1^* & H_2^* & H_3^* & Q_d & c_{1,0}\end{bmatrix}^T.$$

Applying a series of manipulations, the nonlinear model of the network can be expressed in state space form as follows

$$\frac{dx}{dt}=\Gamma\left(x\right)+Z\left(x\right)u\left(t\right), \tag{18}$$

where $\Gamma\left(x_p\right)=\left[\gamma_j\left(x_p\right)\right]\in\mathbb{R}^{13\times 1}$, $Z\left(x\right)=\left[z_{i,j}\left(x\right)\right]\in\mathbb{R}^{13\times 5}$ and their non-zero elements are

$$\gamma_1\left(x\right)=-\frac{A_1gx_4}{L_1}-\frac{x_1^2f\left(x_1,D_1,\varepsilon_1\right)}{2A_1D_1},\ \gamma_2\left(x\right)=\frac{A_2gx_4}{L_2}-\frac{x_2^2f\left(x_2,D_2,\varepsilon_2\right)}{2A_2D_2},$$
$$\gamma_3\left(x\right)=\frac{A_3gx_4}{L_3}-\frac{x_3^2f\left(x_3,D_3,\varepsilon_3\right)}{2A_3D_3},\ \gamma_4\left(x\right)=\frac{b^2\left(x_1-x_2-x_3\right)}{A_1gL_1},$$
$$\gamma_5\left(x\right)=\left(-k_1-\frac{4n_{cl}x_1}{D_1^2L_1\pi}\right)x_5,\ \gamma_6\left(x\right)=\frac{4n_{cl}x_1\left(x_5-x_6\right)}{D_1^2L_1\pi}-k_1x_6,$$
$$\gamma_7\left(x\right)=\frac{4n_{cl}x_1\left(x_6-x_7\right)}{D_1^2L_1\pi}-k_1x_7,\ \gamma_8\left(x\right)=\frac{4n_{cl}x_2\left(x_7-x_8\right)}{D_2^2L_2\pi}-k_1x_8,$$

$$\gamma_9(x)=\frac{4n_{cl}x_2(x_8-x_9)}{D_2^2L_2\pi}-k_1x_9,\ \gamma_{10}(x)=\frac{4n_{cl}x_2(x_9-x_{10})}{D_2^2L_2\pi}-k_1x_{10},$$

$$\gamma_{11}(x)=\frac{4n_{cl}x_3(-x_{11}+x_7)}{D_3^2L_3\pi}-k_1x_{11},\ \gamma_{12}(x)=\frac{4n_{cl}(x_{11}-x_{12})x_3}{D_3^2L_3\pi}-k_1x_{12},$$

$$\gamma_{13}(x)=\frac{4n_{cl}(x_{12}-x_{13})x_3}{D_3^2L_3\pi}-k_1x_{13},\ z_{1,1}(x)=\frac{A_1g}{L_1},\ z_{2,2}(x)=-\frac{A_2g}{L_2},$$

$$z_{3,3}(x)=-\frac{A_3g}{L_3},\ z_{4,4}(x)=-\frac{b^2}{A_1gL_1},\ z_{5,5}(x)=\frac{4n_{cl}}{D_1^2L_1\pi}x_1.$$

2.4 Linear Approximant of the Benchmark WDN

In order to develop the linear approximant of the nonlinear model (18), the nominal points of all system variables are considered to be constant and satisfying steady flow behavior in the conduits. Let $\bar{u}_j$ ($j=1,\ldots,5$) be the nominal values of the inputs of the system and $\bar{x}_i$ ($i=1,\ldots,13$) be the corresponding nominal values of the state variables. Furthermore, let $\bar{u}$ and $\bar{x}$ be the vectors of nominal values of the inputs and the state variable. The operating vector of the dynamics of the system is denoted as the pair $\bar{o}=(\bar{u},\bar{x})$, where its elements satisfy the following equality

$$\Theta(\bar{x},\bar{u})=0, \tag{19}$$

where $\Theta(\bar{x},\bar{u})=\Gamma(\bar{x})+B(\bar{x})\bar{u}$. Applying a series of manipulations upon (19), it can be verified that

$$\bar{u}_1=\bar{x}_4+\frac{L_1\bar{x}_1^2f(\bar{x}_1,D_1,\varepsilon_1)}{2A_1^2D_1g},\ \bar{u}_2=\bar{x}_4-\frac{L_2\bar{x}_2^2f(\bar{x}_2,D_2,\varepsilon_2)}{2A_2^2D_2g},$$

$$\bar{u}_3=\bar{x}_4-\frac{L_3\bar{x}_3^2f(\bar{x}_3,D_3,\varepsilon_3)}{2A_3^2D_3g},\ \bar{u}_4=\bar{x}_1-\bar{x}_2-\bar{x}_3,\ \bar{x}_5=\frac{4n_{cl}\bar{u}_5\bar{x}_1}{D_1^2k_1L_1\pi+4n_{cl}\bar{x}_1},$$

$$\bar{x}_6=\frac{4n_{cl}\bar{x}_1}{D_1^2k_1L_1\pi+4n_{cl}\bar{x}_1}\bar{x}_5,\ \bar{x}_7=\frac{16n_{cl}^2\bar{x}_1^2}{\left(D_1^2k_1L_1\pi+4n_{cl}\bar{x}_1\right)^2}\bar{x}_5,$$

$$\bar{x}_8=\frac{256n_{cl}^4\bar{u}_5\bar{x}_1^3\bar{x}_2}{\left(D_1^2k_1L_1\pi+4n_{cl}\bar{x}_1\right)^3\left(D_2^2k_1L_2\pi+4n_{cl}\bar{x}_2\right)},\ \bar{x}_9=\frac{4n_{cl}\bar{x}_2}{D_2^2k_1L_2\pi+4n_{cl}\bar{x}_2}\bar{x}_8,$$

$$\bar{x}_{10}=\frac{16n_{cl}^2\bar{x}_2^2}{\left(D_2^2k_1L_2\pi+4n_{cl}\bar{x}_2\right)^2}\bar{x}_8,\ \bar{x}_{11}=\frac{256n_{cl}^4\bar{u}_5\bar{x}_1^3\bar{x}_3}{\left(D_1^2k_1L_1\pi+4n_{cl}\bar{x}_1\right)^3\left(D_3^2k_1L_3\pi+4n_{cl}\bar{x}_3\right)},$$

$$\bar{x}_{12}=\frac{4n_{cl}\bar{x}_3}{D_3^2k_1L_3\pi+4n_{cl}\bar{x}_3}\bar{x}_{11},\ \bar{x}_{13}=\frac{16n_{cl}^2\bar{x}_3^2}{\left(D_3^2k_1L_3\pi+4n_{cl}\bar{x}_3\right)^2}\bar{x}_{11}.$$

The flow constraints in (17) are also valid for the respective flow nominal values, i.e. it holds that

$$\left(\overline{x}_1 \geq 0\right) \wedge \left(\overline{x}_2 \geq 0\right) \wedge \left(\overline{x}_3 \geq 0\right) \wedge \left(\overline{u}_5 \geq 0\right). \tag{20}$$

Regarding the solvability of the nonlinear system in (19), with respect to $\overline{x}$, it suffices that

$$\operatorname{rank}\left\{J_s\left(\overline{x},\overline{u}\right)\right\} = 13, \tag{21}$$

where $J_s\left(\overline{x},\overline{u}\right) = \partial\Theta\left(\overline{x},\overline{u}\right)/\partial\overline{x}$. This matrix can be expressed in terms of its elements as $J_s\left(\overline{x},\overline{u}\right) = \left[\left(j_s\right)_{i,j}\right] \in \mathbb{R}^{13\times 13}$. Applying a series of manipulations, it can be verified that the nonzero elements of $J_s\left(\overline{x},\overline{u}\right)$ are

$$\left(j_s\right)_{j,j} = -\frac{\overline{x}_j}{2A_j D_j}\left(2f\left(\overline{x}_j, D_j, \varepsilon_j\right) + \overline{x}_j \left.\frac{\partial f\left(\lambda, D_j, \varepsilon_j\right)}{\partial \lambda}\right|_{\lambda=\overline{x}_j}\right) \quad ; \; j = 1,2,3,$$

$$\left(j_s\right)_{1,4} = -\frac{A_1 g}{L_1}, \; \left(j_s\right)_{2,4} = \frac{A_2 g}{L_2}, \; \left(j_s\right)_{3,4} = \frac{A_3 g}{L_3},$$

$$\left(j_s\right)_{4,1} = -\left(j_s\right)_{4,2} = -\left(j_s\right)_{4,3} = \frac{b^2}{A_1 g L_1}, \; \left(j_s\right)_{5,1} = \frac{4n_{cl}\left(\overline{u}_5 - \overline{x}_5\right)}{D_1^2 L_1 \pi}, \; \left(j_s\right)_{5,5} = -k_1 - \frac{4n_{cl}\overline{x}_1}{D_1^2 L_1 \pi},$$

$$\left(j_s\right)_{6,1} = \frac{4n_{cl}\left(\overline{x}_5 - \overline{x}_6\right)}{D_1^2 L_1 \pi}, \; \left(j_s\right)_{6,5} = \frac{4n_{cl}\overline{x}_1}{D_1^2 L_1 \pi}, \; \left(j_s\right)_{6,6} = -k_1 - \frac{4n_{cl}\overline{x}_1}{D_1^2 L_1 \pi},$$

$$\left(j_s\right)_{7,1} = \frac{4n_{cl}\left(\overline{x}_6 - \overline{x}_7\right)}{D_1^2 L_1 \pi}, \; \left(j_s\right)_{7,6} = \frac{4n_{cl}\overline{x}_1}{D_1^2 L_1 \pi}, \; \left(j_s\right)_{7,7} = -k_1 - \frac{4n_{cl}\overline{x}_1}{D_1^2 L_1 \pi},$$

$$\left(j_s\right)_{8,2} = \frac{4n_{cl}\left(\overline{x}_7 - \overline{x}_8\right)}{D_2^2 L_2 \pi}, \; \left(j_s\right)_{8,7} = \frac{4n_{cl}\overline{x}_2}{D_2^2 L_2 \pi}, \; \left(j_s\right)_{8,8} = -k_1 - \frac{4n_{cl}\overline{x}_2}{D_2^2 L_2 \pi},$$

$$\left(j_s\right)_{9,2} = \frac{4n_{cl}\left(\overline{x}_8 - \overline{x}_9\right)}{D_2^2 L_2 \pi}, \; \left(j_s\right)_{9,8} = \frac{4n_{cl}\overline{x}_2}{D_2^2 L_2 \pi}, \; \left(j_s\right)_{9,9} = -k_1 - \frac{4n_{cl}\overline{x}_2}{D_2^2 L_2 \pi},$$

$$\left(j_s\right)_{10,2} = \frac{4n_{cl}\left(\overline{x}_9 - \overline{x}_{10}\right)}{D_2^2 L_2 \pi}, \; \left(j_s\right)_{10,9} = \frac{4n_{cl}\overline{x}_2}{D_2^2 L_2 \pi}, \; \left(j_s\right)_{10,10} = -k_1 - \frac{4n_{cl}\overline{x}_2}{D_2^2 L_2 \pi},$$

$$\left(j_s\right)_{11,3} = \frac{4n_{cl}\left(\overline{x}_7 - \overline{x}_{11}\right)}{D_3^2 L_3 \pi}, \; \left(j_s\right)_{11,7} = \frac{4n_{cl}\overline{x}_3}{D_3^2 L_3 \pi}, \; \left(j_s\right)_{11,11} = -k_1 - \frac{4n_{cl}\overline{x}_3}{D_3^2 L_3 \pi},$$

$$\left(j_s\right)_{12,3} = \frac{4n_{cl}\left(\overline{x}_{11} - \overline{x}_{12}\right)}{D_3^2 L_3 \pi}, \; \left(j_s\right)_{12,11} = \frac{4n_{cl}\overline{x}_3}{D_3^2 L_3 \pi}, \; \left(j_s\right)_{12,12} = -k_1 - \frac{4n_{cl}\overline{x}_3}{D_3^2 L_3 \pi},$$

$$\left(j_s\right)_{13,3} = \frac{4n_{cl}\left(\overline{x}_{12} - \overline{x}_{13}\right)}{D_3^2 L_3 \pi}, \; \left(j_s\right)_{13,12} = \frac{4n_{cl}\overline{x}_3}{D_3^2 L_3 \pi}, \; \left(j_s\right)_{13,13} = -k_1 - \frac{4n_{cl}\overline{x}_3}{D_3^2 L_3 \pi}.$$

Applying a series of computations, it can be verified that the condition in (21) is satisfied if and only if the following conditions hold true:

i. $\overline{x}_j \neq -\dfrac{D_j^2 k_j L_j \pi}{4 n_{cl}}$ ($j = 1,2,3$),

ii. $\dfrac{1}{L_1^2}(j_s)_{2,2}(j_s)_{3,3} + \dfrac{A_2}{A_1 L_1 L_2}(j_s)_{1,1}(j_s)_{3,3} + \dfrac{A_3}{A_1 L_1 L_3}(j_s)_{1,1}(j_s)_{2,2} \neq 0$.

Obviously, the first condition is true, as the nominal values of the flow rates are constrained by (21) and all physical parameters of the model are positive. Regarding the second condition, it is observed that in the present case, namely the case of turbulent flow, the parameters $(j_s)_{j,j}$ ($j = 1,2,3$) are negative and hence the condition holds true.

The linear approximant of (18) is evaluated to be of the form

$$\frac{d}{dt}\delta x = J_s(\overline{x},\overline{u})\delta x + Z(\overline{x})\delta u(t), \tag{22}$$

where δx is the response of the above linear system for $\delta u = \Delta u = u - \overline{u}$, that approximates $\Delta x = x - \overline{x}$ around the operating point $\overline{o} = (\overline{u},\overline{x})$. Since the nonlinear system in (19) has been proven to be solvable with respect to $\overline{x}$, there exist a nonlinear vector function, mapping the nominal values of the inputs and the nominal values of the states, i.e., $\overline{x} = \sigma(\overline{u})$. Hence, the linear approximant system matrices in (22) can be rewritten as

$$A(\overline{u}) = J_s(\sigma(\overline{u}),\overline{u}),\ B(\overline{u}) = Z(\sigma(\overline{u})).$$

It is observed that A is in lower block triangular form and only the first five rows of B are different than zero, i.e.,

$$A(\overline{u}) = \begin{bmatrix} A_{1,1}(\overline{u}) & 0_{4\times 9} \\ A_{2,1}(\overline{u}) & A_{2,2}(\overline{u}) \end{bmatrix},\quad B(\overline{u}) = \begin{bmatrix} \underset{i=1,2,3,4,5}{\operatorname{diag}} \{b_{i,i}(\overline{u})\} \\ 0_{8\times 5} \end{bmatrix}, \tag{23}$$

where $A_{1,1}(\overline{u}) \in \mathbb{R}^{4\times 4}$, $A_{2,1}(\overline{u}) \in \mathbb{R}^{9\times 4}$ and $A_{2,2}(\overline{u}) \in \mathbb{R}^{9\times 9}$.

3 A Luenberger type Full order Observer for the WDN

Due to technical and economic constraint, it is extremely difficult or even impossible to measure, in real time, all variables of the dynamics of a WDN. Although the volumetric flow rates in various sections, the pressure, and the chlorine concentration in various points of interest, are important for monitoring satisfaction of regulations, only a limited number of sensors can be installed to the system. Flow rate and pressure are typically monitored only at main junctions or boundary points. Chlorine concentration is even harder to measure, in real time. Although it can be measured at some of the monitoring stations, it cannot be measured directly within the conduits themselves. This is due to the intrusive character of chemical sensing and the difficulties in installing effective in-line chlorine sensors that can withstand the operating conditions inside the pipes.

To face the problem of sensing chlorine, a Luenberger type full order observer of the linear approximant in Subsection 2.4, will be designed. A common case, also adopted here, is the case where the only real time measurable variables are the volumetric flow rate in some conduits and the chlorine concentrations in reservoirs. Here, the volumetric flow rates are measured in conduits 2 and 3. Also, the chlorine concentrations are measured at the entrance of reservoirs 2 and 3. Hence, the measurable output vector is the following

$$y_m = C_m x , \tag{24}$$

where $C_m = \left[(c_m)_{i,j} \right] \in \mathbb{R}^{4\times 13}$. The non-zero elements of C_m are $(c_m)_{1,3} = (c_m)_{2,4} = (c_m)_{3,10} = (c_m)_{4,13} = 1$. From (22) and (24) it is observed that $\delta y_m = C_m \delta x$, where δy_m is the response of the measurable outputs of the system for $\delta u = \Delta u = u - \overline{u}$. This response approximates $\Delta y_m = y_m - \overline{y}_m$ around the operating point $\overline{o} = (\overline{u}, \overline{x})$. Using (22) and (24) and applying a series of manipulations, it can be verified that the system is observable, independently of the nominal values of the inputs and the state variables. Hence, the observer poles can arbitrarily be selected to satisfy specific design criteria. The observer is selected to be of the following full order Luenberger form using the variations of the inputs and the measurement outputs of the nonlinear system, see [1] and [2],

$$\Im : \frac{d}{dt}\delta\hat{x}(t) = F(\overline{u})\delta\hat{x}(t) + G(\overline{u})\Delta y_m(t) + M(\overline{u})\Delta u(t), \delta\hat{x}(0-) = \delta\hat{x}_0 , \tag{25}$$

where $F(\overline{u}) \in \mathbb{R}^{13\times 13}$, $G(\overline{u}) \in \mathbb{R}^{13\times 4}$ and $M(\overline{u}) \in \mathbb{R}^{13\times 5}$ are appropriate observer matrices to be selected by the designer. Here, the goal of the observer is to compute a vector $\delta\hat{x}(t)$ that will estimate Δx, in an appropriate region of Δu. It is important to mention that the system matrices of the observer are function matrices of the operating points. Similarly to [1] and [2], the matrices F and M are selected to be

$$F(\overline{u}) = A(\overline{u}) - G(\overline{u}) C_m , \tag{26}$$

$$M(\overline{u}) = B(\overline{u}) . \tag{27}$$

The elements of G are to be selected by the designer such that the eigenvalues of F are appropriately adjusted. Regarding selection of the elements of G, applying series of computations upon the system matrices in (25) it can readily be observed that the characteristic polynomial of the linear approximant can be written as a product of two polynomials in the form

$$p(s) = p_f(s)\,p_c(s), \tag{28}$$

where $p_f(s)$ is a fourth order polynomial, depending upon the parameters of the fluid dynamics, and $p_c(s)$ is a ninth order polynomial, depending upon the chlorine concentration parameters. For the observer to have the polynomial factorial form (28) as well as to facilitate the selection of the parameters of the matrix G, the observer matrix is selected to be of the following block diagonal form

$$G(\bar{u}) = \begin{bmatrix} G_{1,1}(\bar{u}) & 0_{4\times 2} \\ 0_{9\times 2} & G_{2,2}(\bar{u}) \end{bmatrix}, \tag{29}$$

where $G_{1,1}(\bar{u}) = \left[\left(g_{1,1}\right)_{i,j}\right] \in \mathbb{R}^{4\times 2}$ and $G_{2,2}(\bar{u}) = \left[\left(g_{2,2}\right)_{i,j}\right] \in \mathbb{R}^{9\times 2}$. Also, upon expressing the measurable output matrix C_m in the following block diagonal form

$$C_m = \begin{bmatrix} C_{m,1} & 0_{2\times 9} \\ 0_{2\times 4} & C_{m,2} \end{bmatrix}, \tag{30}$$

the observer characteristic polynomial is factored as follows

$$p_o(s) = \det\left(sI_{13} - F(\bar{u})\right) = p_{o,f}(s)\,p_{o,c}(s), \tag{31}$$

where

$$p_{o,f}(s) = \det\left(sI_4 - A_{1,1}(\bar{u}) + G_{1,1}(\bar{u})C_{m,1}\right), \tag{32}$$

$$p_{o,c}(s) = \det\left(sI_4 - A_{2,2}(\bar{u}) + G_{2,2}(\bar{u})C_{m,2}\right). \tag{33}$$

Let $\pi_{f,j}$ ($j = 1,\ldots,4$) are the roots of $p_f(s)$ and $\pi_{c,i}$ ($i = 1,\ldots,9$) are the roots of $p_c(s)$. Without loss of generality, assume that $\left|\mathrm{Re}\left(\pi_{f,j}\right)\right| \le \left|\mathrm{Re}\left(\pi_{f,j+1}\right)\right|$ ($j = 1,2,3$) and that $\left|\mathrm{Re}\left(\pi_{c,i}\right)\right| \le \left|\mathrm{Re}\left(\pi_{c,i+1}\right)\right|$ ($i = 1,\ldots,8$).

In what follows, the observer polynomial roots are restricted to satisfy the following constraints:

- The roots of $p_{o,f}(s)$ and $p_{o,c}(s)$ are real and negative, i.e., $p_{o,f}(s) = \prod_{j=1}^{4}\left(s - (\pi_{o,f})_j\right)$ and $p_{o,c}(s) = \prod_{i=1}^{9}\left(s - (\pi_{o,c})_i\right)$, where $(\pi_{o,f})_j < 0$ ($j = 1,\ldots,4$) and $(\pi_{o,c})_i < 0$ ($i = 1,\ldots,9$).
- The roots of $p_{o,f}(s)$ and $p_{o,c}(s)$ are ordered and have a minimum distance between them being equal to γ i.e. it holds that $\left|(\pi_{o,f})_{j+1}\right| - \left|(\pi_{o,f})_j\right| > \gamma$ ($j = 1,2,3$) and $\left|(\pi_{o,c})_{i+1}\right| - \left|(\pi_{o,c})_i\right| > \gamma$.

- Regional per pole stability is achieved, i.e. it holds that $\left|\left(\pi_{o,f}\right)_j\right| > \lambda\left|\mathrm{Re}\left(\pi_{f,j}\right)\right|$ and $\left|\left(\pi_{o,c}\right)_i\right| > \lambda\left|\mathrm{Re}\left(\pi_{c,i}\right)\right|$ where $\lambda > 0$.

The parameters γ and λ are to be selected by the observer designer. It can readily be observed that the observer pole placement problem has multiple solutions. In what follows, the pole placement problem will be solved using the observer degrees of freedom appearing in the first columns of $G_{1,1}\left(\overline{u}\right)$ and $G_{2,2}\left(\overline{u}\right)$. Clearly, the solution will be a function of the remaining degrees of freedom. These degrees of freedom as well as the values of the poles can be determined so that other design requirements are achieved.

It is important to mention that the above observer design procedure implies that:

i. the linear approximant in (22) is fully known, a priori or through an identification / parameter determination procedure (indicative see [1] and [2])
ii. the output and input variables of the process are measured in real time, and
iii. the operating trajectory of the nonlinear process is known inside an appropriate operating region.

The operating trajectory is the set of all operating points satisfying (19). The third implication means that the set of all these points is known to the designer, inside a range of the participating variables.

4 A Heuristic Approach toward Determination of the Observer Degrees of Freedom

Toward determination of the degrees of freedom of the observer, a metaheuristic approach, having similarities to those in [24] and [25], will be used. Applying elementary computations, it can readily be observed that the frequency response dynamics of the observer in (25) is of the form

$$\delta\hat{X}\left(s\right) = \Phi\left(s\right)\left[G\left(\overline{u}\right)\Delta Y_m\left(s\right) + M\left(\overline{u}\right)\Delta U\left(s\right)\right] + \Phi\left(s\right)\delta\hat{x}_0\,, \tag{34}$$

where $\Phi\left(s\right) = \left(sI_{13} - F\left(\overline{u}\right)\right)^{-1} = \left[\varphi_{i,j}\left(s\right)\right] \in \mathbb{R}\left(s\right)^{13\times 13}$ is the observer resolvent matrix and $\delta\hat{X}\left(s\right)$, $\Delta Y_m\left(s\right)$ and $\Delta U\left(s\right)$ denote the Laplace transforms of $\delta\hat{x}\left(t\right)$, $\Delta y_m\left(t\right)$ and $\Delta u\left(t\right)$, respectively. Clearly, if the observer's degrees of freedom satisfy the constraints imposed in Section 3, stability is achieved, guaranteeing that the free response of the observer tends to zero. Define the free observer parameter vector

$$\chi = \left[\chi_1 \quad \cdots \quad \chi_{26}\right]^T = \left[\left(\pi_{o,f}\right)_1 \quad \cdots \quad \left(\pi_{o,f}\right)_4 \;\vdots\; \left(\pi_{o,c}\right)_1 \quad \cdots \quad \left(\pi_{o,c}\right)_9 \;\vdots\right.$$
$$\left.\vdots\; \left(g_{1,1}\right)_{1,2} \quad \cdots \quad \left(g_{1,1}\right)_{4,2} \;\vdots\; \left(g_{2,2}\right)_{1,2} \quad \cdots \quad \left(g_{2,2}\right)_{9,2}\right]^T.$$

The elements of χ will be determined so that the influence of the free response to the observer response is attenuated. This attenuation will be achieved by appropriately selecting χ such that the following cost criterion is minimized

$$J\left(\chi,\bar{u}\right)=\max_{i=1,\ldots,13}\left\{\int_0^\infty \sum_{j=1}^{13}\left|h_{i,j}\left(t\right)\right|dt\right\}, \tag{35}$$

where $h_{i,j}\left(t\right)=\mathcal{L}^{-1}\left\{\varphi_{i,j}\left(s\right)\right\}$ is the $\{i,j\}$ element of the transition matrix of the observer dynamics in (25) and where $\mathcal{L}^{-1}\{\bullet\}$ denotes the inverse Laplace transform of the argument transfer function. Clearly, the optimization procedure must be executed separately at each operating point.

The main idea of the algorithm is to define a search area for the observer parameters and after series of computations to contract to suboptimal values, satisfying the observer constraints. The search area for each parameter is defined by the center value, let $\left(\chi_j\right)_c$ ($j=1,\ldots,26$), and the respective half-width $\left(\chi_j\right)_w$. The optimization algorithm presented in [24] and [25] is modified as follows:

Metaheuristic Optimization Algorithm

Initialization

- Set search area bounds using center values and half-widths of parameters $\left(\chi_j\right)_c$ and $\left(\chi_j\right)_w$ ($j=1,\ldots,26$).
- Define the performance criterion in (35).
- Set the observer pole thresholds λ and γ.
- Set the optimization parameters n_{loop} , n_{rep} , $n_{total}\in\mathbb{N}$
- Set the convergence parameter ε.

Algorithm

S0: Set $i_{\max}=0$ and $n_{min}=\infty$.

S1: Define the search space $\left(\chi_j\right)_c-\left(\chi_j\right)_w\le\chi_j\le\left(\chi_j\right)_c+\left(\chi_j\right)_w$ ($j=1,\ldots,26$).

S2: Set $i_1=0$.

S3: Set $i_1=i_1+1$.

S4: Set $i_2=0$.

S5: Set $i_{\max}=i_{\max}+1$. If $i_{\max}>n_{total}$ go to S15.

S6: Set $i_2=i_2+1$.

S7: Randomly choose a vector of parameters $\chi_{i_2}=\left[\left(\chi_1\right)_{i_2}\quad\cdots\quad\left(\chi_{26}\right)_{i_2}\right]^T$ within the search space and let $\chi_j=\left(\chi_j\right)_{i_2}$.

S8: Check if the constraints presented in Section 3 are satisfied. If they are not satisfied, go to S7.

S9: Determine $J_{i_2}=J\left(\chi,\bar{u}\right)$

S10: If $i_2 < n_{loop}$, then go to S5.

S11: Find $J_{i_1,\min} = \min\left\{J_{i_2}, i_2 = 1,\ldots,n_{loop}\right\}$ and the corresponding observer parameters $\left(\chi_j\right)_{i_1}$ ($j = 1,\ldots,26$).

S12: If $i_1 = n_{rep}$ then determine the observer parameters, $\left(\chi_j\right)_{\min}$ and $\left(\chi_j\right)_{\max}$ corresponding to $J_{\min} = \min\left\{J_{i_1,\min}, i_1 = 1,\ldots,n_{rep}\right\}$ and $J_{\max} = \max\{J_{i_i,\min}, i_1 = 1,\ldots,n_{rep}\}$, respectively. Else go to S3

S13: If $J_{\min} < n_{min}$, set $n_{min} = J_{\min}$, $\left(\chi_j\right)_c = \left(\chi_j\right)_{\min}$ and $\left(\chi_j\right)_w = \left|\left(\chi_j\right)_{\min} - \left(\chi_j\right)_{\min}\right|$ ($j = 1,\ldots,26$).

S14: If $\min\limits_{j=1,\ldots,26}\left\{\left|\left(\chi_j\right)_w / \left(\chi_j\right)_c\right|\right\} > \varepsilon$ go to S1.

S15: Set $\chi_j = \left(\chi_j\right)_{\min}$ ($j = 1,\ldots,26$).

5 Determination of the Observer Operating Areas and Switching Mechanism

5.1 Target Operating Areas

It is important to mention once more that the metaheuristic algorithm, presented in Section 4, produces observer parameters corresponding to a given operating point. The next step is to determine the operating area of the derived observer derived, namely the area where the observer behaves satisfactorily. To do so, define the following five-dimensional spheroid

$$\sum_{j=1}^{5}\left(\frac{\tilde{u}_j - \bar{u}_j}{\bar{u}_j}\right)^2 = R^2 , \tag{36}$$

where $\tilde{u}_j$ denotes the steady state value of u_j ($j = 1,\ldots,5$) during a step wise transition, $\bar{u}_j$ denotes, as already mentioned, the nominal values of the input corresponding to an observer of the form in (24), defining the respective coordinate (in the five dimensional space) of the center of the spheroid and R denotes the radius of the spheroid. Let $\tilde{x}_i$ ($i = 1,\ldots,13$) denote the steady state value of the state variable x_i corresponding to $\tilde{u}_j$ ($j = 1,\ldots,5$). Let $\tilde{u}$ and $\tilde{x}$ be the steady state input and state variable vectors corresponding to the above transition. Note that $\tilde{x}_i$ and $\tilde{u}_j$ can be determined following a similar procedure to that presented in Subsection 2.5 for the determination of the operating point. Finally, let $\tilde{x}_e$ be the estimation of $\tilde{x}$ derived through the observer in (25), where

$$\tilde{x}_e = \bar{x} - F\left(\bar{u}\right)^{-1}\left[G\left(\bar{u}\right)C_m\left(\tilde{x} - \bar{x}\right) + M\left(\bar{u}\right)\left(\tilde{u} - \bar{u}\right)\right]. \tag{37}$$

Define the augmented vectors $\tilde{\zeta} = \begin{bmatrix} \tilde{x}^T & \tilde{u}^T \end{bmatrix}^T$, $\bar{\zeta} = \begin{bmatrix} \bar{x}^T & \bar{u}^T \end{bmatrix}^T$ and $\tilde{\zeta}_e = \begin{bmatrix} \tilde{x}_e^T & \tilde{u}^T \end{bmatrix}^T$ as well as the normalization matrix

$$W = \begin{bmatrix} \mathrm{diag}\left\{\bar{x}_j^{-1}\right\} & 0_{13\times 5} \\ 0_{5\times 13} & \mathrm{diag}\left\{\bar{u}_i^{-1}\right\} \end{bmatrix}. \tag{38}$$

Based on the above definition, consider the following normalized estimation steady state error metric:

$$\varepsilon_{ss} = \sqrt{\frac{\left[W\left(\tilde{x}-\tilde{x}_e\right)\right]^T\left[W\left(\tilde{x}-\tilde{x}_e\right)\right]}{\left[W\left(\tilde{x}-\bar{x}\right)\right]^T\left[W\left(\tilde{x}-\bar{x}\right)\right]}} \times 100\% \tag{39}$$

The target area for the operating point $\bar{o} = \left(\bar{u}, \bar{x}\right)$ is defined as the maximum radius of the spheroid in (36), such that all input transitions from the operating point to a new steady state value inside the spheroid, result in $\varepsilon_{ss} < \varepsilon_{ss,\max}$, where $\varepsilon_{ss,\max}$ is a positive parameters selected by the observer designer. Note that the transitions do not necessarily start from the operating point, since the steady state value of the state variables depends only on the steady state value of the input and not the initial point. Clearly, this procedure must be repeated for a sufficiently large number of points to ensure that the desired area is covered by target operating regions that satisfy the dense web principle. Following a similar procedure to that in [1], the idea lies first in generating a uniform grid or nominal values of the inputs and next, in determining, for each set of inputs, the corresponding observer and after checking if the dense web principle [1] is satisfied. If it is satisfied, then superfluous points are eliminated. If it is not satisfied, the areas that remain uncovered are determined and additional points in the middle of the uncovered areas are selected.

5.2 Switching Between Observers

As already mentioned, the observer matrices depend upon the operating point of the system belonging to a prespecified set of operating points of the system. Let O be the set of nominal operating points, as described in the previous subsection, satisfying the dense web principle. Around each nominal operating point, the nonlinear system is approximated by a respective linear approximant, while the respective observer matrices can be evaluated as described in Sections 3 and 4. These observers constitute a, so-called, bank of observers. Assume that the bank of observers includes the observers $\Im_1, \ldots, \Im_\mu$. For proper operation it is evident that a switching mechanism that appropriately enables the operation of appropriately chosen observer of the bank is necessary. Considering that the performance outputs of the system are measurable in real time and that the trajectory of the nonlinear process is known, an approach based upon the convergence of the measurable variable of the system to their target values is proposed. Define the time dependent convergence metric

$$\varepsilon_c\left(t\right)=\sqrt{\frac{\left(y_m\left(t\right)-C_m\tilde{x}\right)^T\left(y_m\left(t\right)-C_m\tilde{x}\right)}{\left[C_m\left(\tilde{x}-\overline{x}\right)\right]^T\left[C_m\left(\tilde{x}-\overline{x}\right)\right]}}\times 100\% \,. \tag{40}$$

Here, during each transition, switching between observers will take place whenever the convergence metric reaches a threshold $\varepsilon_s \in \mathbb{R}^+$, i.e. when $\varepsilon_c\left(t\right)=\varepsilon_s$.

6 Simulation Results

In order to demonstrate the performance of the proposed switching observer scheme, let $A_1=0.0079\left[\mathrm{m}^2\right]$, $A_2=0.0079\left[\mathrm{m}^2\right]$, $A_3=0.0028\left[\mathrm{m}^2\right]$, $L_1=62\left[\mathrm{m}\right]$, $L_2=124\left[\mathrm{m}\right]$, $L_3=80\left[\mathrm{m}\right]$, $D_1=0.1\left[\mathrm{m}\right]$, $D_2=0.1\left[\mathrm{m}\right]$, $D_3=0.06\left[\mathrm{m}\right]$, $\varepsilon_1=0.0035\left[-\right]$, $\varepsilon_2=0.0035\left[-\right]$, $\varepsilon_3=0.0058\left[-\right]$, $g=\left[\mathrm{m/s}^2\right]$, $\rho=\left[\mathrm{Kg/m}^3\right]$, $\mu=0.0011\left[\mathrm{Pa\,s}\right]$, $n_{cl}=3\left[-\right]$, $k_1=0.1\left[\mathrm{h}^{-1}\right]$, $b=1200\left[\mathrm{m/s}\right]$, $\lambda_1=0.308642\left[-\right]$, $\lambda_2=6.9\left[-\right]$, $\lambda_3=3.7\left[-\right]$ and $\lambda_4=1.11\left[-\right]$. Consider the uniform grid of nominal values of the inputs presented in Table 1.

Table 1. Operating point trajectory

#	$\overline{u}_1$ $\left[\mathrm{m}\right]$	$\overline{u}_2$ $\left[\mathrm{m}\right]$	$\overline{u}_3$ $\left[\mathrm{m}\right]$	$\overline{u}_4$ $\left[\mathrm{l/min}\right]$	$\overline{u}_5$ $\left[\mathrm{mg/l}\right]$
1	20.0000	17.0000	14.0000	360.0000	2.0000
2	20.5263	16.8947	14.1053	356.8421	1.9737
3	21.0526	16.7895	14.2105	353.6842	1.9474
4	21.5789	16.6842	14.3158	350.5263	1.9211
5	22.1053	16.5789	14.4211	347.3684	1.8947
6	22.6316	16.4737	14.5263	344.2105	1.8684
7	23.1579	16.3684	14.6316	341.0526	1.8421
8	23.6842	16.2632	14.7368	337.8947	1.8158
9	24.2105	16.1579	14.8421	334.7368	1.7895
10	24.7368	16.0526	14.9474	331.5789	1.7632
11	25.2632	15.9474	15.0526	328.4211	1.7368
12	25.7895	15.8421	15.1579	325.2632	1.7105
13	26.3158	15.7368	15.2632	322.1053	1.6842
14	26.8421	15.6316	15.3684	318.9474	1.6579
15	27.3684	15.5263	15.4737	315.7895	1.6316
16	27.8947	15.4211	15.5789	312.6316	1.6053
17	28.4211	15.3158	15.6842	309.4737	1.5789
18	28.9474	15.2105	15.7895	306.3158	1.5526
19	29.4737	15.1053	15.8947	303.1579	1.5263
20	30.0000	15.0000	16.0000	300.0000	1.5000

Using the above sets of nominal values of the inputs as well as the results of Subsection 2.5, the respective steady state values for the state variables may be determined.

To determine the observer matrices corresponding to the above operating conditions, the analytic / metaheuristic approach presented in Sections 3 and 4 will be used. In particular, for all operating points let $\gamma = 0.01$, $\lambda = 1.1$, $\varepsilon = 0.01$, $n_{loop} = 1000$, $n_{rep} = 30$, $n_{total} = 10^8$ and

$$\left(\chi_j\right)_c = \frac{\lambda+5}{2}\left|\mathrm{Re}\left(\pi_{f,j}\right)\right| \text{ and } \left(\chi_j\right)_w = \frac{3\lambda+5}{2}\left|\mathrm{Re}\left(\pi_{f,j}\right)\right| \text{ for } j = 1,\ldots,4,$$

$$\left(\chi_j\right)_c = \frac{\lambda+5}{2}\left|\mathrm{Re}\left(\pi_{c,i}\right)\right| \text{ and } \left(\chi_j\right)_w = \frac{3\lambda+5}{2}\left|\mathrm{Re}\left(\pi_{c,i}\right)\right| \text{ for } j = 5,\ldots,13,$$

$$\left(\chi_j\right)_c = 0 \text{ and } \left(\chi_j\right)_w = 50 \text{ for } j = 14,\ldots,26.$$

Using the above parameters in conjunction to the metaheuristic algorithm in Section 4, the observer matrix degrees of freedom, per operating point, are determined. Based on these results and applying series of computations, the operating area per nominal value set may be derived. Setting $\varepsilon_{ss,\max} = 5\%$, the five-dimensional spheroid radii presented in Table 2 are derived.

Table 2. Spheroid Radii per Operating Point

#	R	#	R
1	0.0603	11	0.2184
2	0.0833	12	0.2065
3	0.1043	13	0.1837
4	0.1292	14	0.2080
5	0.1466	15	0.2121
6	0.1696	16	0.2169
7	0.1828	17	0.2191
8	0.1789	18	0.2209
9	0.1838	19	0.2493
10	0.2452	20	0.2541

One can easily observe from the data presented in Table 2, an increasing trend for the radius. Although there exists an anomaly in the intermediate portion, as will be shown later, it does not impact the performance of the switching scheme significantly and is most likely due to the metaheuristic algorithm having converged to a local minimum for the particular operating points.

An additional observation that can be made is that the target areas are overlapping and consequently, to implement an observer switching scheme as described previously, not all points need to be used. Applying series of computations, it can be observed that it suffices to use operating points 1, 8 and 16, covering the entire desired region. Indicatively, in Figures 2 to 11 the projection of the 5-dimensional region (per operating point) to 2-dimensional surfaces are presented, demonstrating overlapping areas where switching between observers may take place. The ten plots provide a distinct image of the way in which five-dimensional coordinates, as defined by the variables u_1 to u_5, pattern when plotted in two-dimensional planes. Every one of the ten plots shows three color-coded domains for operating points 1, 8 and 16 (1 – cyan, 8 – green, 16-red) associated with the respective accuracy regions. Amongst the projections, in the $u_1 - u_2$ plane clusters are clearly aligned along the u_1 axis with increasingly widening spread from cyan to red indicating separation and structure. Other projections based on u_1, also indicate the gradient structure, but with growing amounts of overlap. Projections based on u_2 to u_5 indicate higher overlap and less separation.

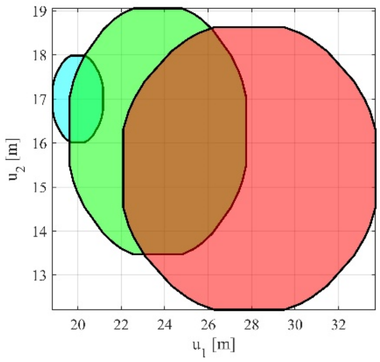

Fig. 2. Projection on the $u_1 - u_2$ plane.

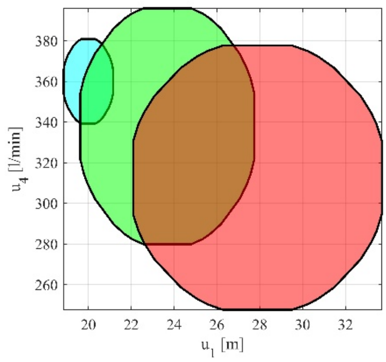

Fig. 4. Projection on the $u_1 - u_4$ plane.

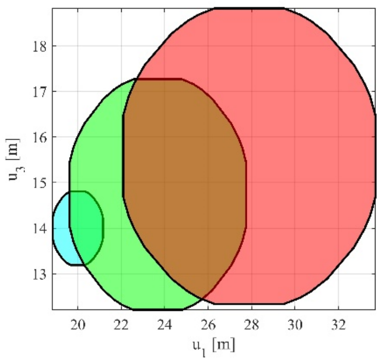

Fig. 3. Projection on the $u_1 - u_3$ plane.

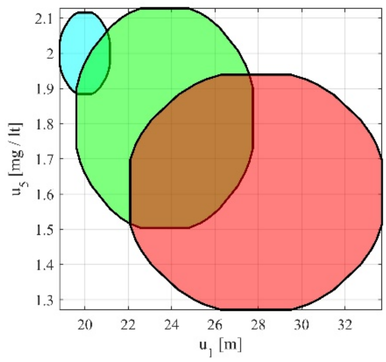

Fig. 5. Projection on the $u_1 - u_5$ plane.

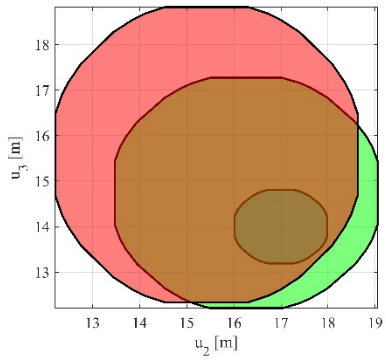

Fig. 6. Projection on the $u_2 - u_3$ plane.

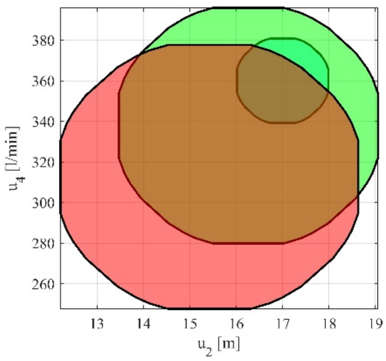

Fig. 7. Projection on the $u_2 - u_4$ plane.

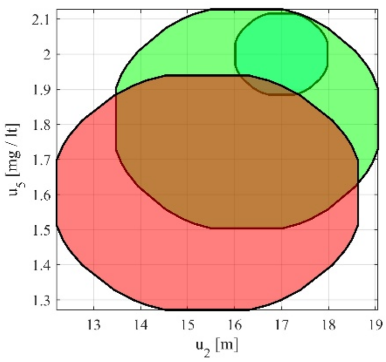

Fig. 8. Projection on the $u_2 - u_5$ plane.

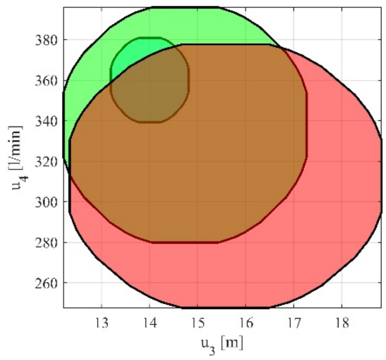

Fig. 9. Projection on the $u_3 - u_4$ plane.

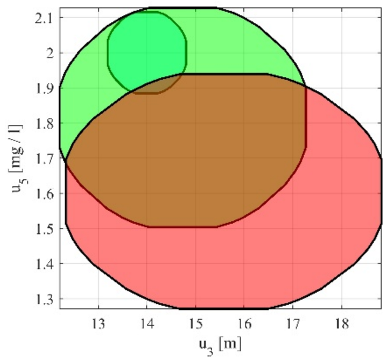

Fig. 10. Projection on the $u_3 - u_5$ plane.

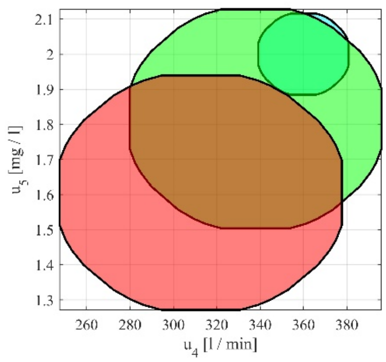

Fig. 11. Projection on the $u_4 - u_5$ plane.

In order to demonstrate the performance of the switching observer consider the following transitions:

- Initial Point: $\overline{u}_1 = 19.7556[\mathrm{m}]$, $\overline{u}_2 = 17.0289[\mathrm{m}]$, $\overline{u}_3 = 14.0429[\mathrm{m}]$, $\overline{u}_4 = 360[\mathrm{l/min}]$, $\overline{u}_5 = 2.0039[\mathrm{mg/lt}]$

- Transition Point 1: $\bar{u}_1 = 20.7163[\text{m}]$, $\bar{u}_2 = 16.7226[\text{m}]$, $\bar{u}_3 = 14.0429[\text{m}]$, $\bar{u}_4 = 354[\text{l/min}]$, $\bar{u}_5 = 1.9697[\text{mg/lt}]$
- Transition Point 2: $\bar{u}_1 = 24.7883[\text{m}]$, $\bar{u}_2 = 15.8112[\text{m}]$, $\bar{u}_3 = 14.9878[\text{m}]$, $\bar{u}_4 = 324[\text{l/min}]$, $\bar{u}_5 = 1.7221[\text{mg/lt}]$
- Target Point: $\bar{u}_1 = 27.8408[\text{m}]$, $\bar{u}_2 = 15.4377[\text{m}]$, $\bar{u}_3 = 15.7097[\text{m}]$, $\bar{u}_4 = 312[\text{l/min}]$, $\bar{u}_5 = 1.5826[\text{mg/lt}]$

Note that transitions u_1 to u_4 from point to point will be assumed to take place smoothly and not in step form. This is a common approach in closed conduits and water distribution networks to prevent water hammer effects, which can potentially damage infrastructure. In Figures 12 to 24, the response of the nonlinear model in (18) in conjunction to the response of the switching observer, for all state variables, is presented. Overall, the observer is highly accurate with negligible deviations that are visible in only a few instances. Regarding the non-measurable variables, in Figure 12, the volumetric flow rate through conduit 1 is presented and shows a nearly ideal match between the system response and the observer estimate. The estimation curve closely tracks the system curve, both in steady-state operation as well as under sudden changes when switching takes place. This shows that the observer is well-tuned for this conduit's dynamics, providing fast convergence and zero steady-state error. In Figure 15, the pressure head at the point of conduit junction is presented. The head pressure estimation is very close to tracing the system response. However, there is a temporary mismatch during the step changes, where estimation is slightly behind the system response. However, the estimation approaches the correct value, demonstrating that the observer is still reasonably accurate. The estimation of chlorine concentrations (see Figures 16, 17, 19, 20, 22 and 23) show that the observer performs satisfactorily for all parts of the conduits being observed. The estimated concentrations follow the actual system responses accurately, following their steady-state levels and their dynamic transitions, with high accuracy. Minor deviations are observed in the steeply sloping (observer switch points) (e.g., Figure 18) that are caused by the observer's slower convergence in these regions. Regarding estimation of the measurable variables, they are practically identical to the respective measurements.

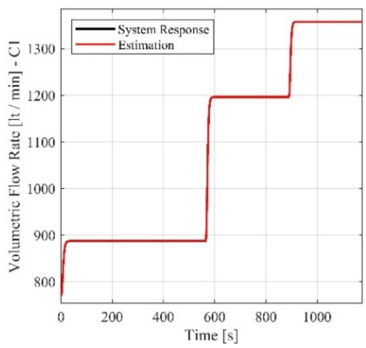

Fig. 12. Estimation of x_1 vs model response.

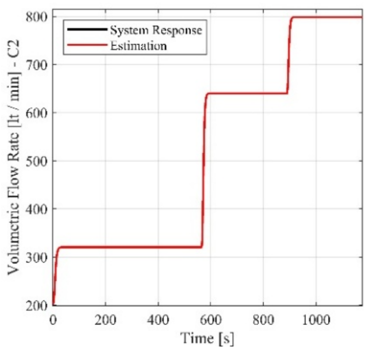

Fig. 13. Estimation of x_2 vs model response.

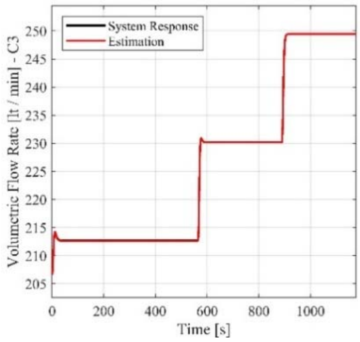

Fig. 14. Estimation of x_3 vs model response.

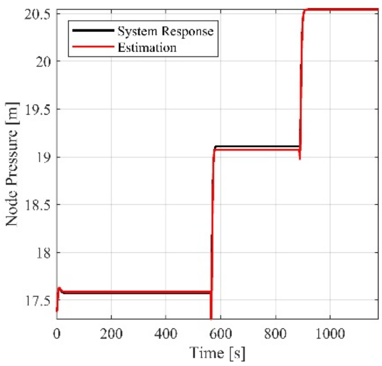

Fig. 15. Estimation of x_4 vs model response.

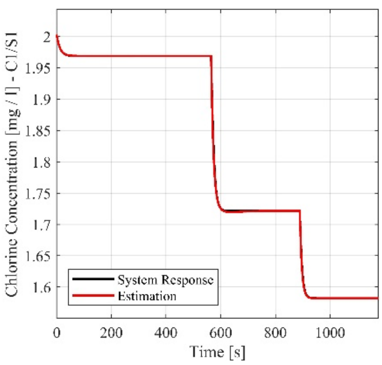

Fig. 16. Estimation of x_5 vs model response.

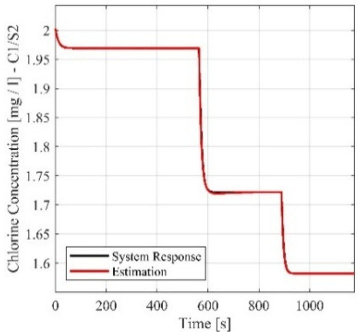

Fig. 17. Estimation of x_6 vs model response.

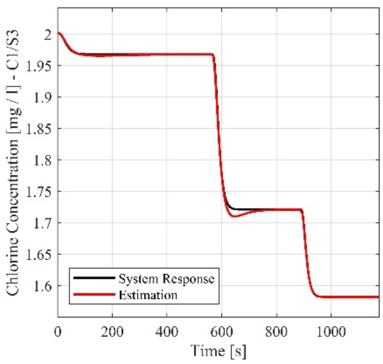

Fig. 18. Estimation of x_7 vs model response.

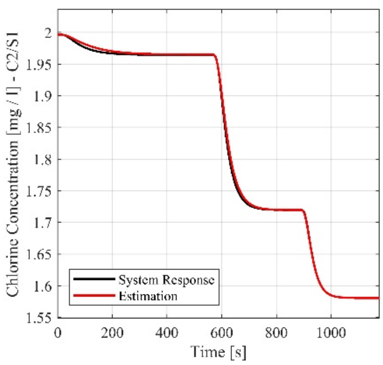

Fig. 19. Estimation of x_8 vs model response.

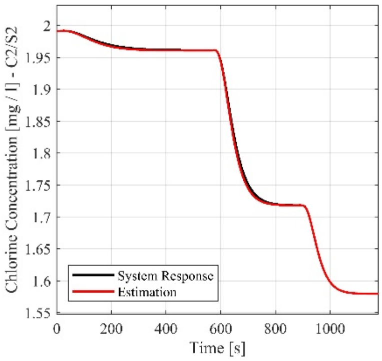

Fig. 20. Estimation of x_9 vs model response.

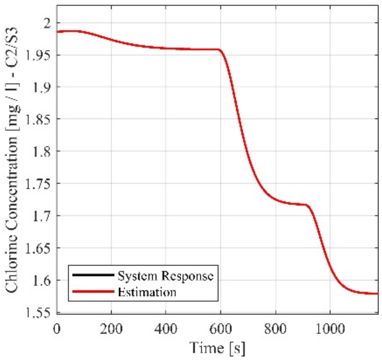

Fig. 21. Estimation of x_{10} vs model response.

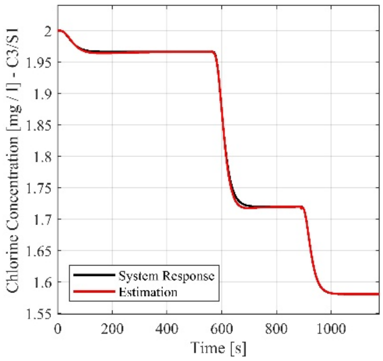

Fig. 22. Estimation of x_{11} vs model response.

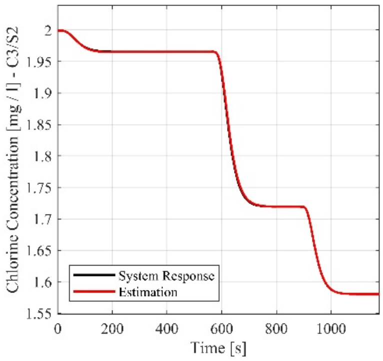

Fig. 23. Estimation of x_{12} vs model response.

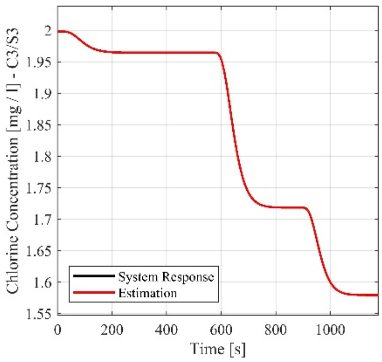

Fig. 24. Estimation of x_{13} vs model response.

7 Conclusions

In the present paper, a novel design approach for chlorine soft sensors in primary WDNs, employing a bank of linear safe switching observers has been presented. The method has employed a nonlinear dynamic approximation of the PDE-based fluid and chlorine transport dynamics and a linear approximant of the nonlinear approximation about selected operating points. The observer parameters have been optimized with a metaheuristic algorithm. Finally, a rule-based data-driven switching has been adopted to switch observers in real time. Computational experiments showed that the proposed method provides reliable and accurate chlorine concentration estimates under various operating conditions.

Future research will focus on enhancing the observer's resilience. Toward this goal, adaptive learning mechanisms and machine learning techniques to adjust observer parameters, in response to model uncertainties and unmodeled dynamics, will be developed. Finally, experimental validation will be performed to evaluate the operational feasibility and scalability of the suggested solution within actual water networks.

References

1. Kouvakas, N.D., Koumboulis, F.N., Fragkoulis, D.G., Fragulis, G.F.: Metaheuristic Procedures for the Determination of a Bank of Switching Observers toward Soft Sensor Design with Application to an Alcoholic Fermentation Process. Mathematics 11(23), 4733 (2023).
2. Koumboulis, F.N., Fragkoulis, D.G., Kouvakas, N.D., Feidopiasti, A.: Soft Sensor Design via Switching Observers. Sensors 23(4), 2114 (2023).
3. Alencar, G.M.R.d., Fernandes, F.M.L., Moura Duarte, R., Melo, P.F.d., Cardoso, A.A., Gomes, H.P., & Villanueva, J.M.M. (2024). A Soft Sensor for Flow Estimation and Uncertainty Analysis Based on Artificial Intelligence: A Case Study of Water Supply Systems. Automation, 5(2), 106–127.
4. Gomes, D.E., Espírito Santo, A., & Páscoa, J. (2024). Artificial Neural Network SoftSensor for Water Distribution Networks. In: Proceedings of IECON 2024 – 50th Annual Conference of the IEEE Industrial Electronics Society, Chicago, IL, USA.
5. Lima, R.P.G., Mauricio Villanueva, J.M., Gomes, H.P., & Flores, T.K.S. (2022). Development of a Soft Sensor for Flow Estimation in Water Supply Systems Using Artificial Neural Networks. Sensors, 22(8), 3084.
6. Djerioui, M., Bouamar, M., Ladjal, M., & Zerguine, A. (2019). Chlorine soft sensor based on extreme learning machine for water quality monitoring. Arabian Journal for Science and Engineering, 44, 2033–2044.
7. Ogundero, M.A., Fashanu, T.A., Agunbiade, F.O., Orolu, K., Yinusa, A.A., Daudu, U.A., & Amuda, M.O.H. (2025). A soft sensor based inference engine for water quality assessment and prediction. Air, Soil and Water Research,
8. Juntunen, P., Liukkonen, M., Lehtola, M.J., & Hiltunen, Y. (2013). Dynamic soft sensors for detecting factors affecting turbidity in drinking water. Journal of Hydroinformatics, 15(2), 416–426.
9. Torres, L., Jiménez-Cabas, J., Ponsart, J.-C., Theilliol, D., Jiménez-Magaña, M.R., & Guzmán, J.E.V. (2024). Pipe roughness calibration approach for water distribution network models using a nonlinear state observer. Results in Engineering, 23, 102713.
10. Vrachimis, S.G., Eliades, D.G., & Polycarpou, M.M. (2018). Leak detection in water distribution systems using hydraulic interval state estimation. In 2018 IEEE Conference on Control Technology and Applications (CCTA) (pp. 565–570). IEEE.
11. Brdys, M.A., Duzinkiewicz, K., Grochowski, M., Rutkowski, T., & Trawicki, D. (2001). Robust estimation of variables and parameters in dynamic water distribution systems. IFAC Proceedings Volumes, 34(8), 179–185.

12. Delgado-Aguiñaga, J.A., Santos-Ruiz, I., Besançon, G., López-Estrada, F.R., & Puig, V. (2022). EKF-based observers for multi-leak diagnosis in branched pipeline systems. Mechanical Systems and Signal Processing, 178, 109198.
13. Santos-Ruiz, I., Bermúdez, J.R., López-Estrada, F.R., Puig, V., Torres, L., & Delgado-Aguiñaga, J.A. (2018). Online leak diagnosis in pipelines using an EKF-based and steady-state mixed approach. Control Engineering Practice, 81, 55–64.
14. Yu, W. (2018). Luenberger Observer Design for Uncertainty Nonlinear Systems. In: Clempner, J.B., Yu, W. (eds) New Perspectives and Applications of Modern Control Theory. Springer.
15. Casolaro, A., Capone, V., Iannuzzo, G., & Camastra, F. (2023). Deep learning for time series forecasting: Advances and open problems. Information, 14(11), 598.
16. Nokhwal, S., Chilakalapudi, P., Donekal, P., Nokhwal, S., Pahune, S., & Chaudhary, A. (2024). Accelerating Neural Network Training: A Brief Review. In Proceedings of the 2024 8th International Conference on Intelligent Systems, Metaheuristics & Swarm Intelligence (ISMSI), 31–35.
17. Rudin, C. (2019). Stop explaining black box machine learning models for high stakes decisions and use interpretable models instead. Nature Machine Intelligence, 1(5), 206–215.
18. Delgado-Aguiñaga, J.A., Besançon, G., Begovich, O., Carvajal, J.E.: Multi-leak diagnosis in pipelines based on Extended Kalman Filter. Control Engineering Practice 49, (2016).
19. Kundu, P.K., Cohen, I.M., Dowling, D.R., Capecelatro, J.: Fluid Mechanics, 7th edn. Academic Press, London (2025).
20. López-Estrada, F.-R., Besançon, G., Valencia-Palomo, G., Torres, L., Hernández, H.-R.: Modeling and Simulation of a Hydraulic Network for Leak Diagnosis. Mathematical and Computational Applications 23(4), 70 (2018).
21. Haaland, S.E. (1983). Simple and Explicit Formulas for the Friction Factor in Turbulent Pipe flow. Journal of Fluids Engineering, 105, 89-90.
22. Islam, M.R., Chaudhry, M.H., Clark, R.M.: Inverse Modeling of Chlorine Concentration in Pipe Networks under Dynamic Condition. Journal of Environmental Engineering 123(10), 1033–1039 (1997).
23. Delgado-Aguiñaga, J.A., Besançon, G.: EKF-based leak diagnosis schemes for pipeline networks. IFAC-PapersOnLine 51(24), 723–729 (2018).
24. Drosou, T.C., Kouvakas, N.D., Koumboulis, F.N., Tzamtzi, M.P.: A Mixed Analytic/Metaheuristic Dual Stage Control Scheme Toward I/O Decoupling for a Differential Drive Mobile Robot. In: Farmanbar, M., Tzamtzi, M., Verma, A.K., Chakravorty, A. (eds) Frontiers of Artificial Intelligence, Ethics, and Multidisciplinary Applications. FAIEMA 2023. Springer, Singapore, pp. 197–214 (2024).
25. Kouvakas, N.D., Koumboulis, F.N., Sigalas, J.: A Two Stage Nonlinear I/O Decoupling and Partially Wireless Controller for Differential Drive Mobile Robots. Robotics 13(2), 26 (2024).